

Tutorial: Intro to Scanning Tunneling Microscopy

(STM)
(STS)

UT Austin, Wang Materials Group

Surface Studies by Scanning Tunneling Microscopy

G. Binning, H. Rohrer, Ch. Gerber, and E. Weibel

IBM Zurich Research Laboratory, 8803 Rüschlikon-ZH, Switzerland

(Received 30 April 1982)

Surface microscopy using vacuum tunneling is demonstrated for the first time. Topographic pictures of surfaces on an *atomic scale* have been obtained. Examples of resolved monoatomic steps and surface reconstructions are shown for (110) surfaces of CaIrSn₄ and Au.

PACS numbers: 68.20.+t, 73.40.Gk

<https://dx.doi.org/10.1103/PhysRevLett.49.57>

2 modes of operation: imaging and spectroscopy

- Imaging: constant current, constant height
- Spectroscopy: sweep V_{bias} or vary tip height from sample to obtain I-V

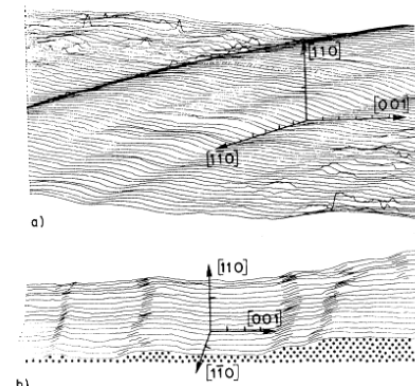
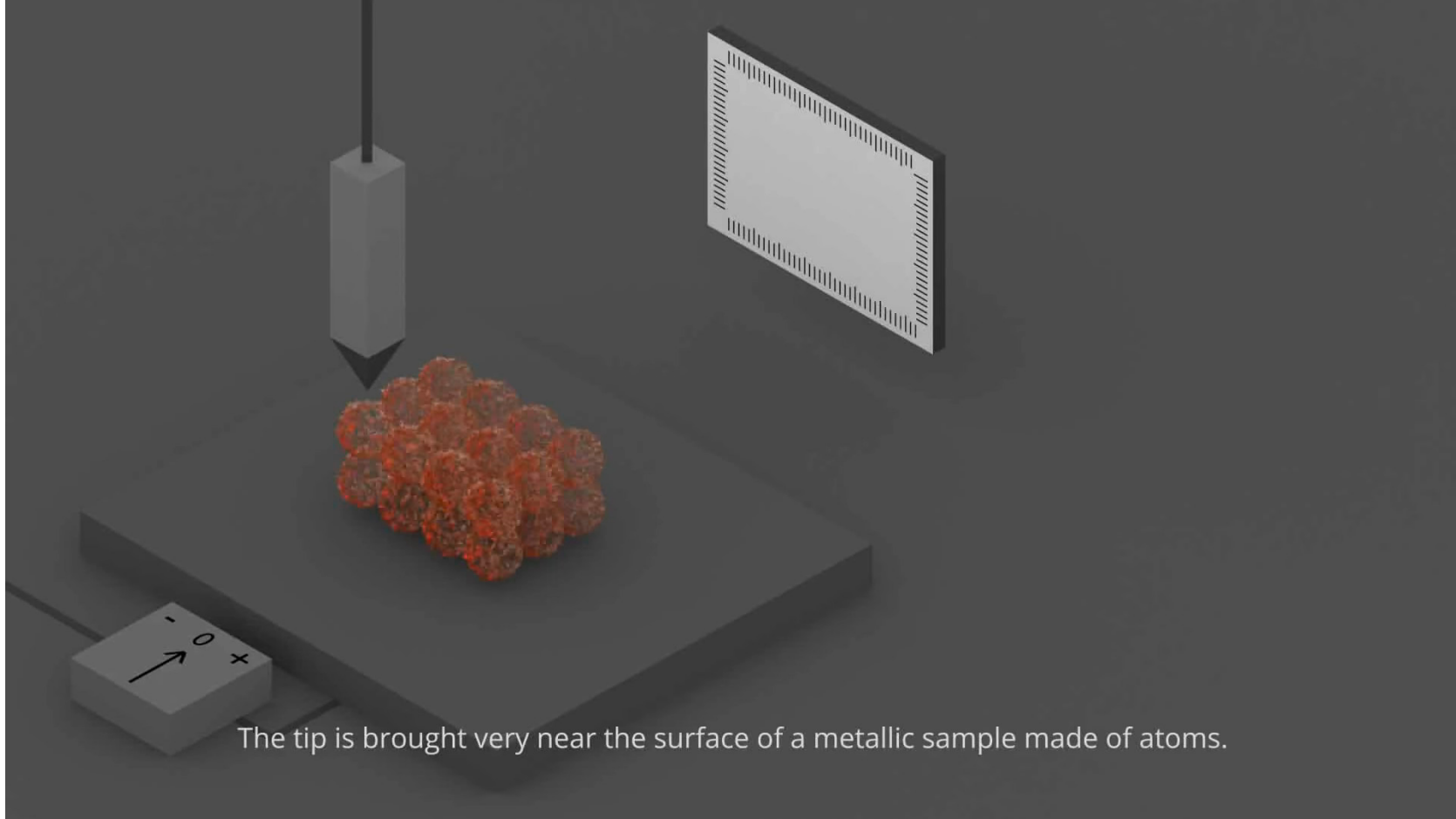


FIG. 3. Two examples of scanning tunneling micrographs of a Au (110) surface, taken at (a) room temperature, and (b) 300 °C after annealing for 20 h at the same temperature (and essentially constant work function). The sensitivity is 10 Å/div everywhere. Because of a small thermal drift, there is some uncertainty in the crystal directions in the surface. In (a), the surface is gently corrugated in the [001] direction, except for a step of four atomic layers (≈ 2 atomic radii) along the [110] direction, as indicated by the discontinuity of the shaded ribbon. The steps in (b), which were always found along the [110] direction, are visualized by the possible positions of the Au atoms (dots).

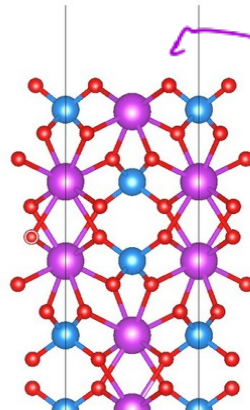


The tip is brought very near the surface of a metallic sample made of atoms.

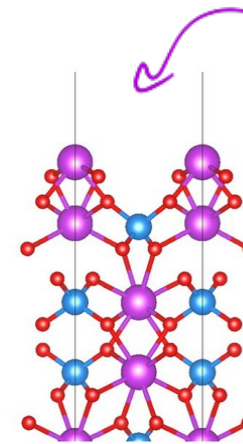
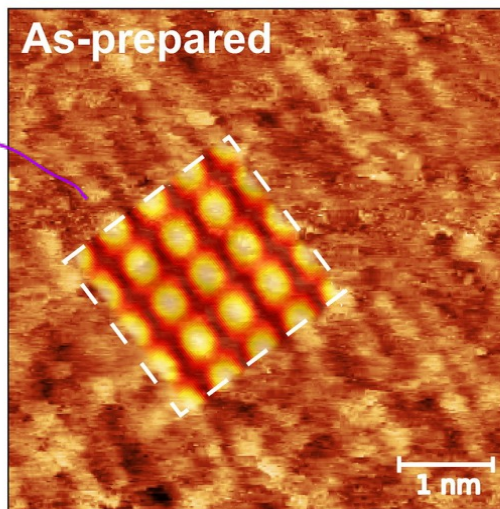
Surface termination impacts photocurrent

We prepared experimental and computational samples with two different surface terminations: as-grown and base-treated (010) surface.

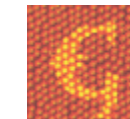
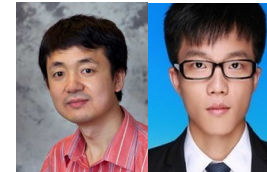
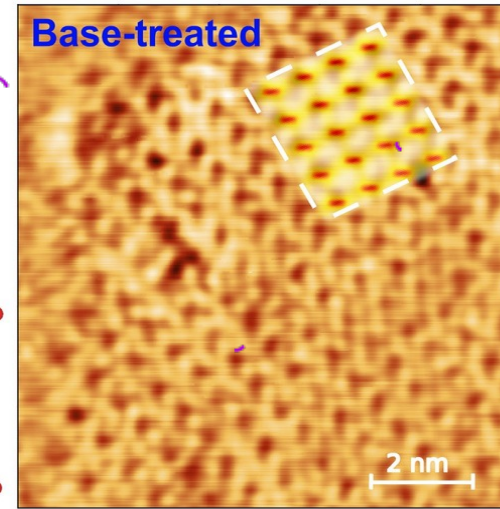
Bi₂O₃



aka “Stoichiometric” surface



aka “Bi-rich” surface



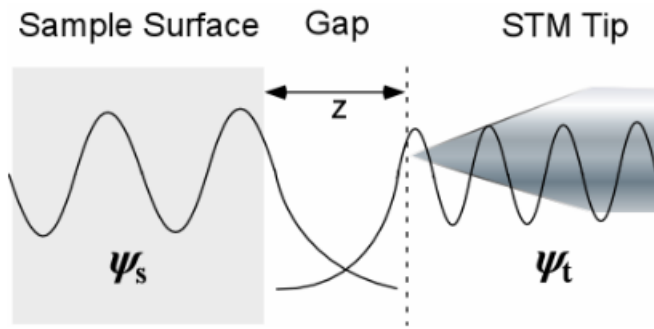


Figure 1: Schematic of STM one-dimensional tunneling configuration.

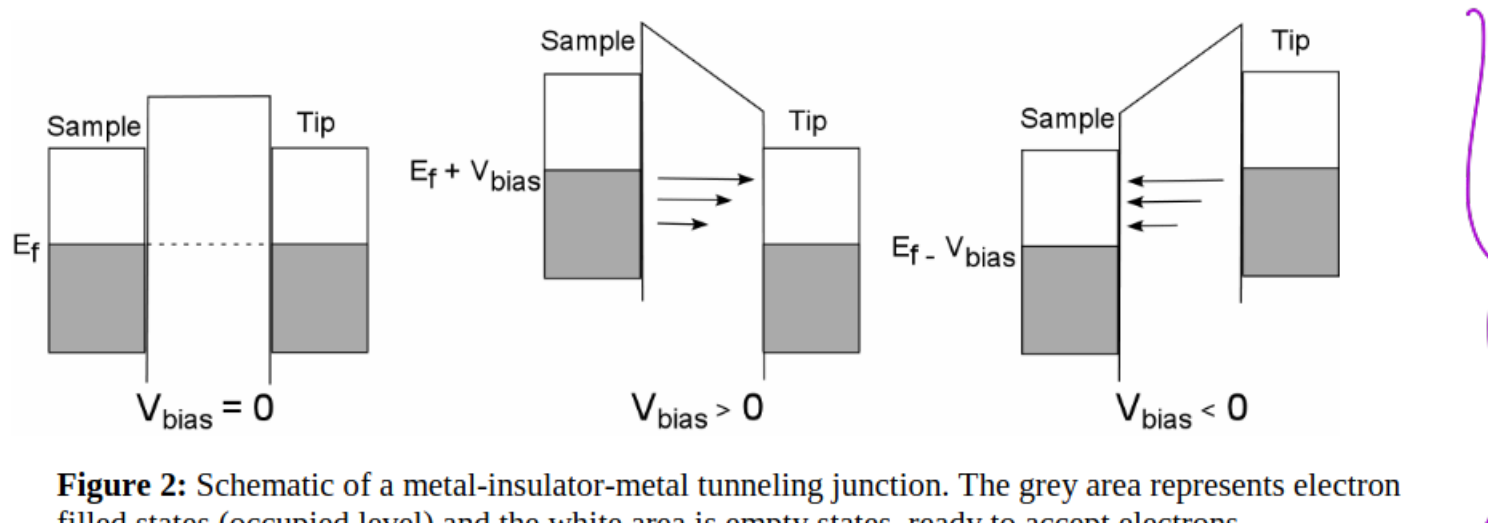


Figure 2: Schematic of a metal-insulator-metal tunneling junction. The grey area represents electron filled states (occupied level) and the white area is empty states, ready to accept electrons (unoccupied level).

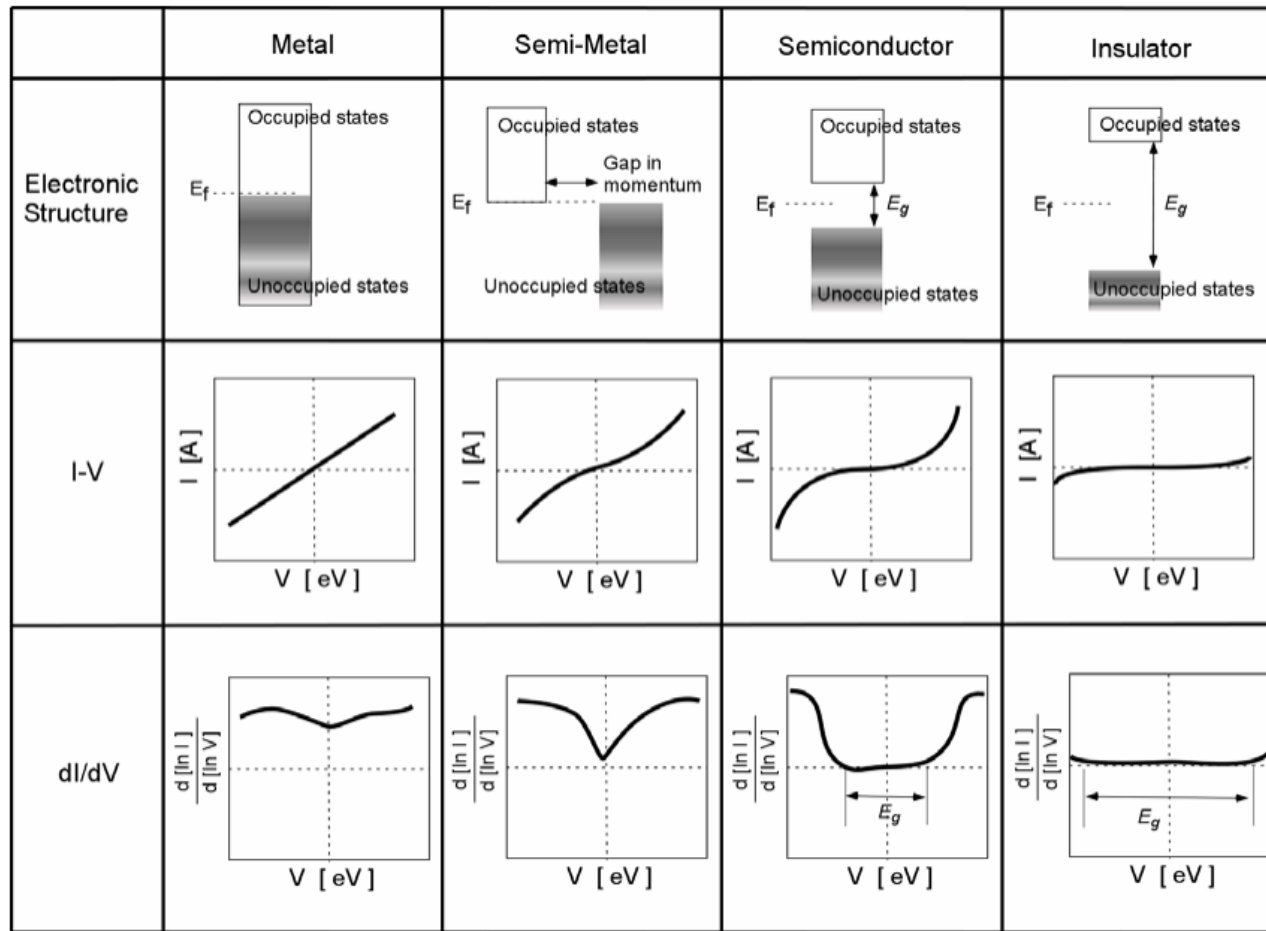
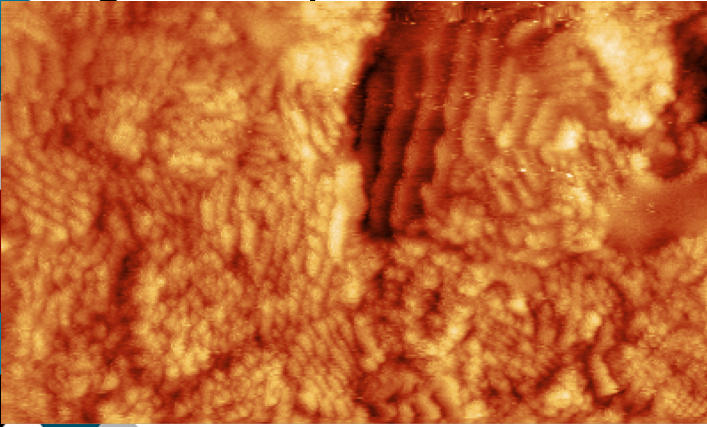


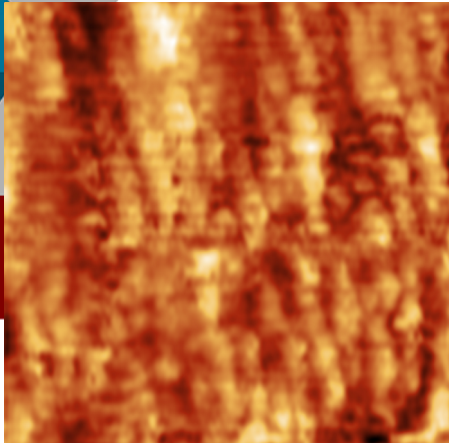
Figure 7: The electronic structures and corresponding IV curves and dI/dV curves of tunneling spectroscopy.

Sampling other areas with STM

As-grown Epitaxial

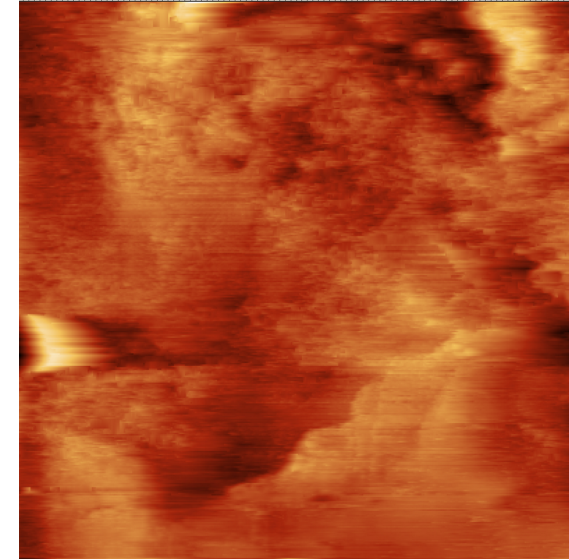


61_1 cropped (~100 x 55 nm)

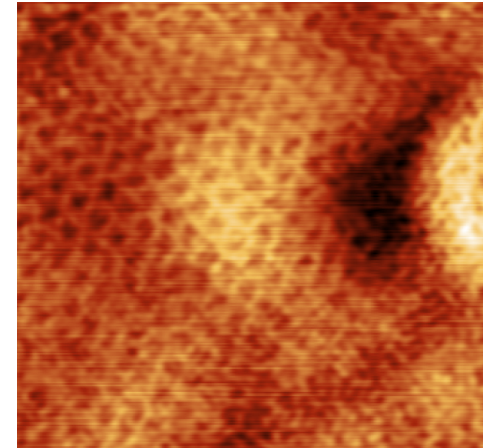


Bi-rich surface

46_3 (~500 x 500 nm)

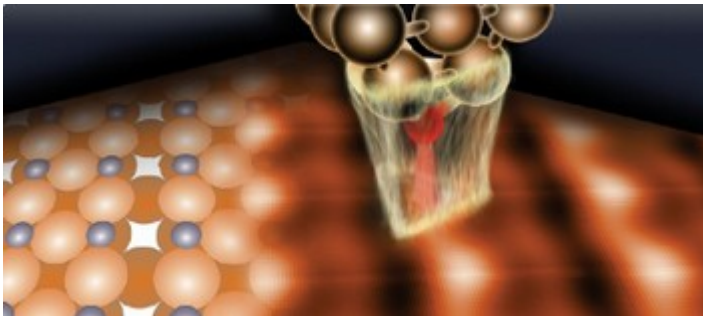


51_4 (~15 x 15 nm)



Simulated STM scans with DFT+U

Determination of surface morphology



Mönig et al. *ACS Nano.* **7**, 10233 (2013).

> Effects of the tip

Quantum ESPRESSO implements:

Tersoff-Haman

$$I \sim \sum_i |\psi_i^{\text{surf}}|^2 \delta(E_i^{\text{surf}} - E_F)$$

Tersoff & Haman. *Phys. Rev. B.* **31**, 805 (1985)

PHYSICAL REVIEW B

VOLUME 31, NUMBER 2

15 JANUARY 1985

Theory of the scanning tunneling microscope

J. Tersoff* and D. R. Hamann
AT&T Bell Laboratories, Murray Hill, New Jersey 07974
(Received 25 June 1984)

We present a theory for tunneling between a real surface and a model probe tip, applicable to the recently developed "scanning tunneling microscope." The tunneling current is found to be proportional to the local density of states of the surface, at the position of the tip. The effective lateral resolution is related to the tip radius R and the vacuum gap distance d approximately as $[(2 \text{ \AA})(R + d)]^{1/2}$. The theory is applied to the 2×1 and 3×1 reconstructions of Au(110); results for the respective corrugation amplitudes and for the gap distance are in all excellent agreement with experimental results of Binnig *et al.* if a 9-\text{\AA} tip radius is assumed. In addition, a convenient approximate calculational method based on atom superposition is tested; it gives reasonable agreement with the self-consistent calculation and with experiment for Au(110). This method is used to test the structure sensitivity of the microscope. We conclude that for the Au(110) measurements the experimental "image" is relatively insensitive to the positions of atoms beyond the first atomic layer. Finally, tunneling to semiconductor surfaces is considered. Calculations for GaAs(110) illustrate interesting qualitative differences from tunneling to metal surfaces.

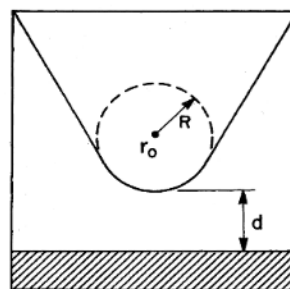


FIG. 1. Schematic picture of tunneling geometry. Probe tip has arbitrary shape but is assumed locally spherical with radius of curvature R , where it approaches nearest the surface (shaded). Distance of nearest approach is d . Center of curvature of tip is labeled r_0 .

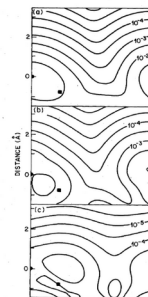
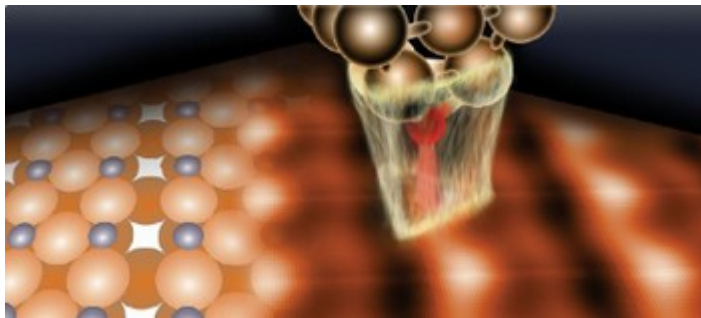


FIG. 4. Projected charge densities at the GaAs(110) surface, in a (110) plane midway between the Ga and As atoms, in units of bohr^{-3} . The vacuum charge density is much smoother in the direction perpendicular to the figure. The three panels show (a) total charge density; (b) charge density within the valence-band edge; (c) charge in states within 1 eV of the conduction-band edge. Positions of the surface atoms, projected into the plane of the figure, are given by circles (As) and squares (Ga). Horizontal direction is (001), vertical is (110).

Simulated STM scans with DFT+U

Determination of surface morphology



Mönig et al. *ACS Nano.* **7**, 10233 (2013).

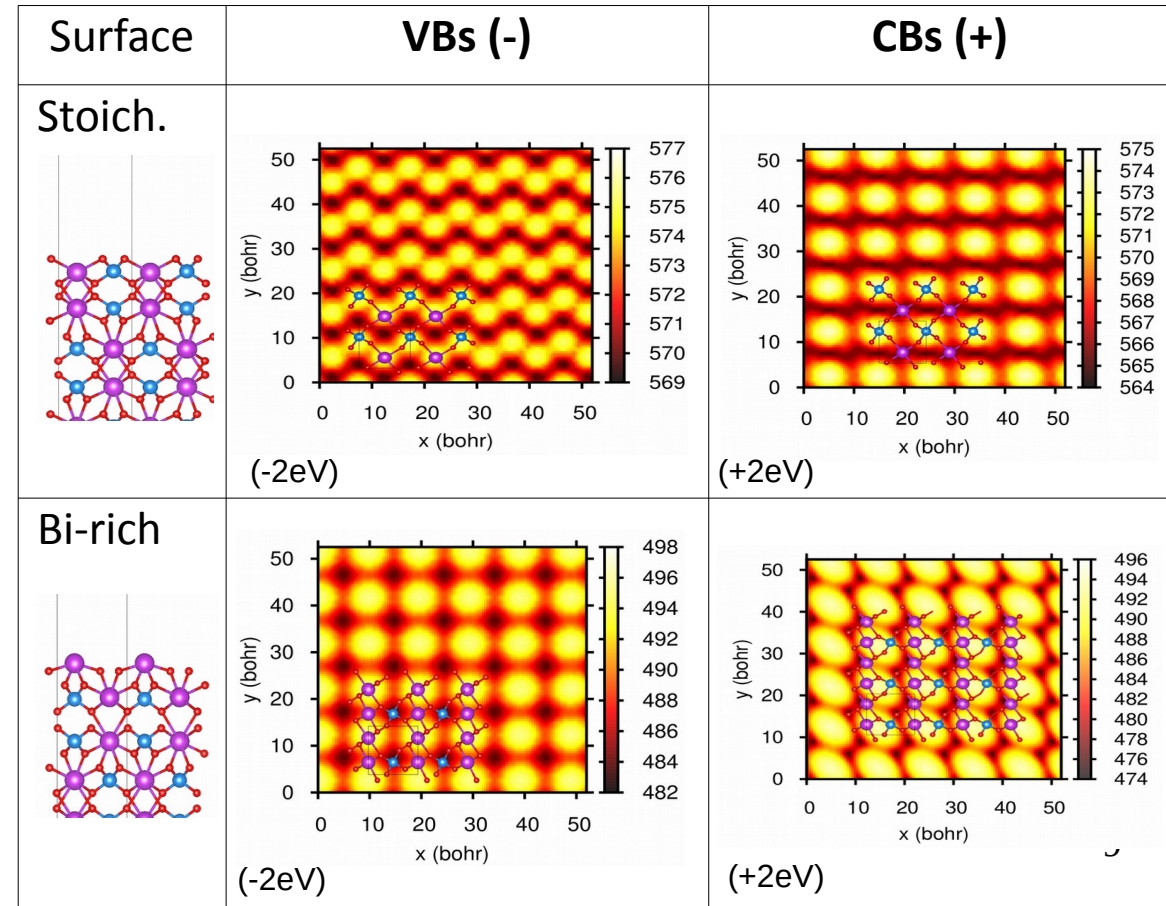
> Effects of the tip

Tersoff-Haman

$$I \sim \sum_i |\psi_i^{\text{surf}}|^2 \delta(E_i^{\text{surf}} - E_F)$$

> LDOS@surf

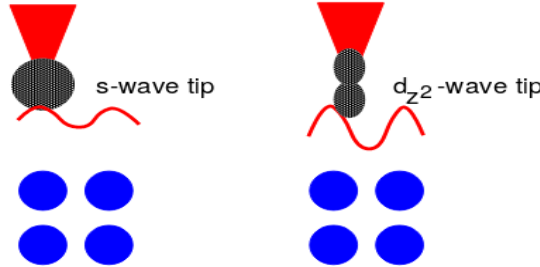
Quantum ESPRESSO implements:
Tersoff & Haman. *Phys. Rev. B.* **31**, 805 (1985)



STM measurements considerations

Beyond Tersoff-Haman method:

- Chen's derivative rules:



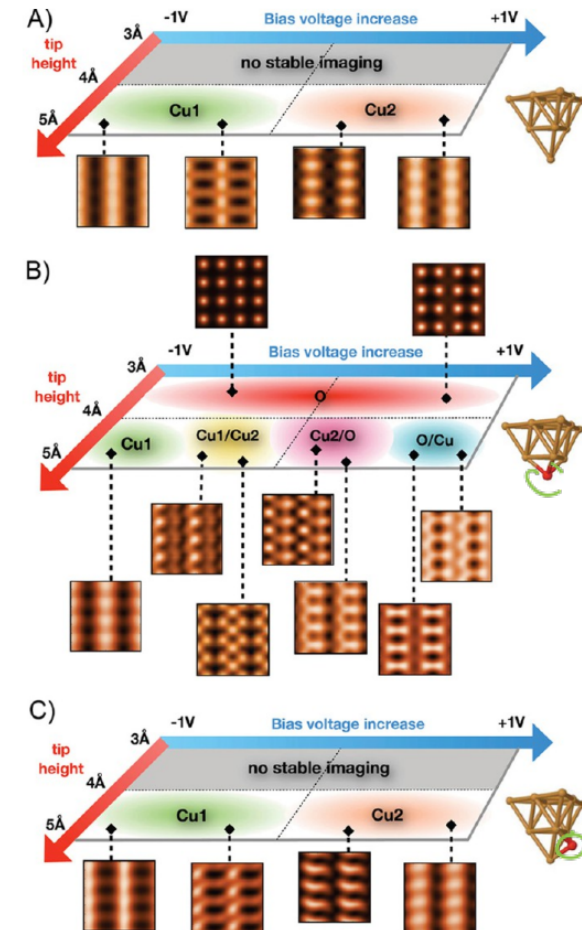
$$\chi_\nu(\mathbf{r}) = \sum C_{\nu\beta} \tilde{Y}_{\nu\beta}$$
$$|M_{\mu\nu}|^2 \sim \left| \sum_\beta \tilde{C}_{\nu\beta} \hat{\partial}_{\nu\beta} \psi_\mu(\mathbf{r}_0) \right|^2$$

- Non-equilibrium Green's functions

Influence of tip & measurement conditions on STM images

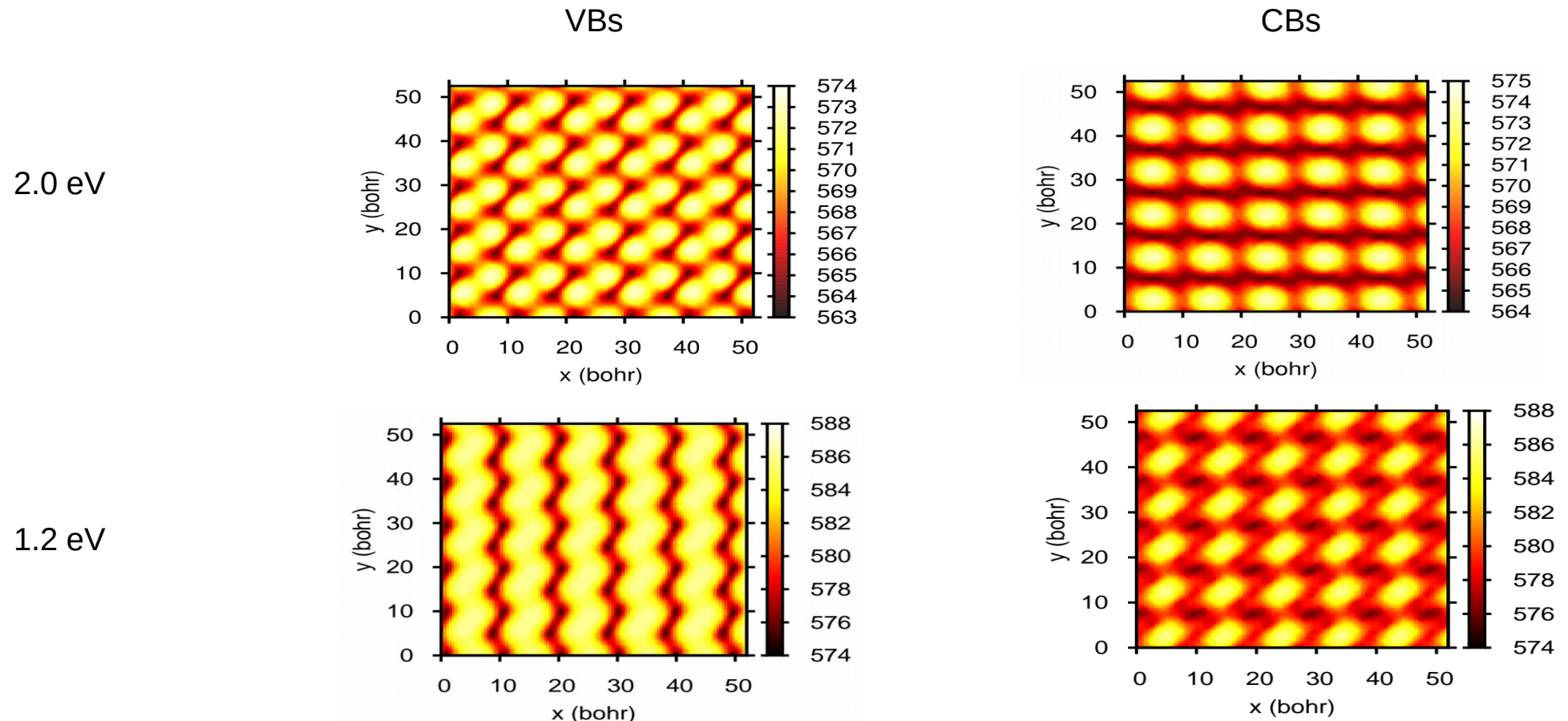
Cu/Cu-O tips over Cu (111) surfaces

Mönig et al. *ACS Nano.* **7**, 10233 (2013).



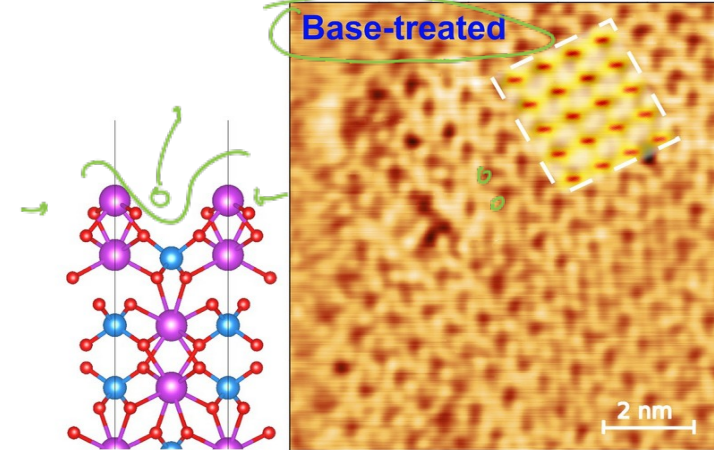
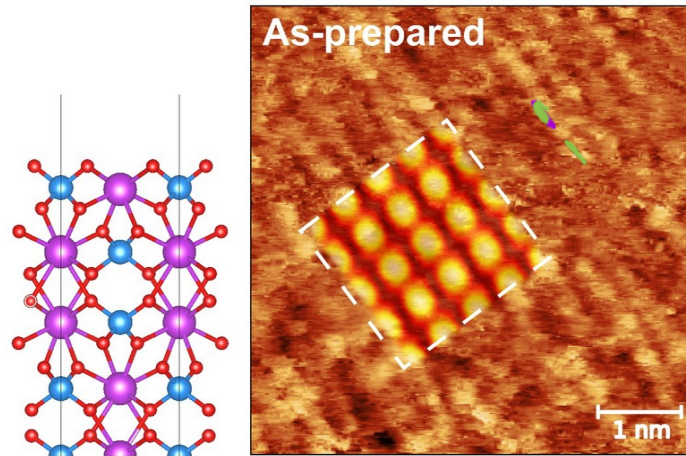
STM: Stoich. BVO (001), LDOS

Influence of sampling bias



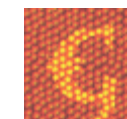
Bringing Theory and Experiment together: STM imaging

Simulated and measured STM images for the as-grown and base-treated (010) surface are in good agreement



	Epitaxial	Simulated
$\Delta_x; \Delta_y (\text{\AA})$	$\sim 4.5\text{--}5.5$	5.17
$\Delta h (\text{\AA})$	$\sim 0.4\text{--}0.6$	0.56

	Epitaxial	Simulated
$\Delta_x; \Delta_y (\text{\AA})$	$\sim 5.0\text{--}6.0$	5.17
$\Delta h (\text{\AA})$	$\sim 0.8\text{--}1.1$	1.54



Analyzed with
Gwyddion

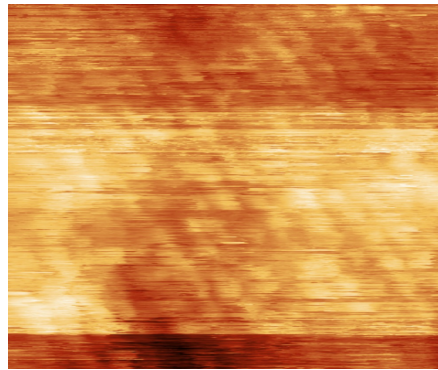
STM image post-processing procedure (Gwyddion)

As grown epitaxial

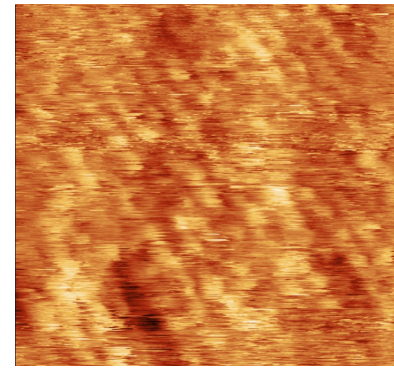
1) Raw Data



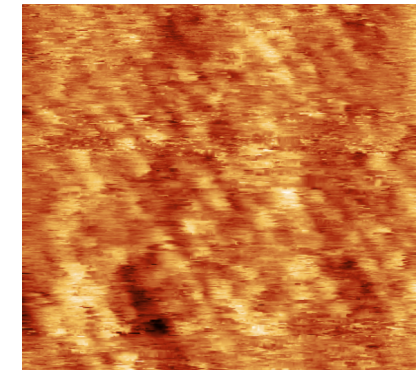
2) Mean plane subtraction



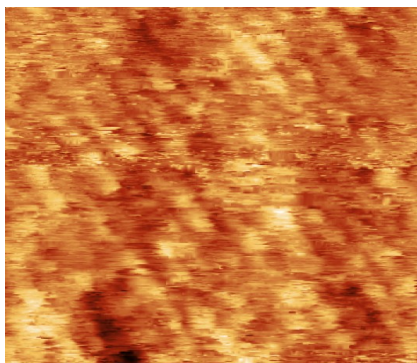
3) Polynomial Align Rows (4th order)



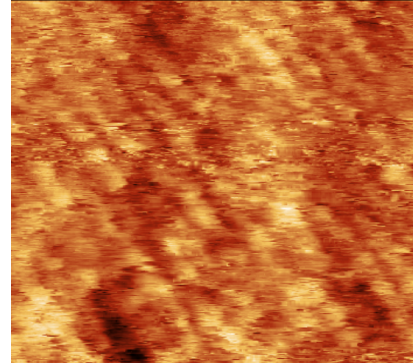
4) Remove Horizontal scars x3



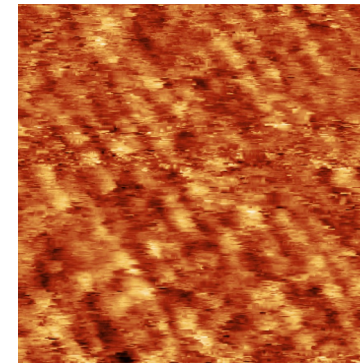
5) Crop image



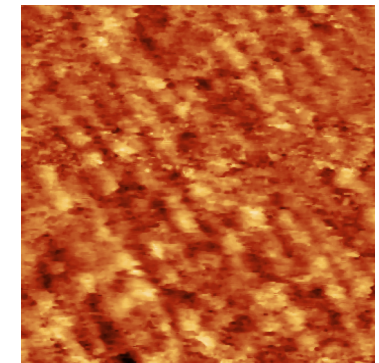
6) 2D FFT



7) Conservative Denoise filter (3px)



8) Median denoise filter (3px)



Introduction to Tunneling

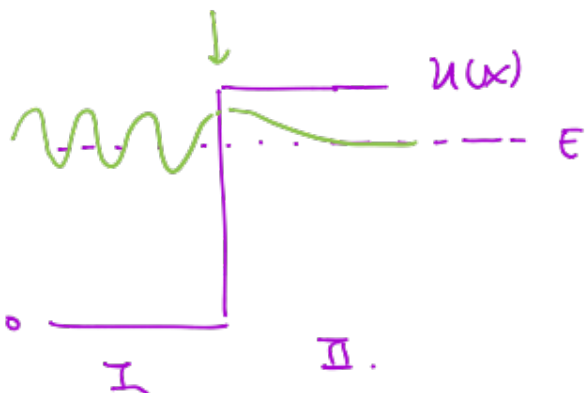
WKB Approximation- the basic idea - Griffiths

↳ Wentzel, Kramers, Brillouin

- * approx solns to time-ind. form of Schrödinger's eq.
- * particularly useful for bound state energies + tunneling rates

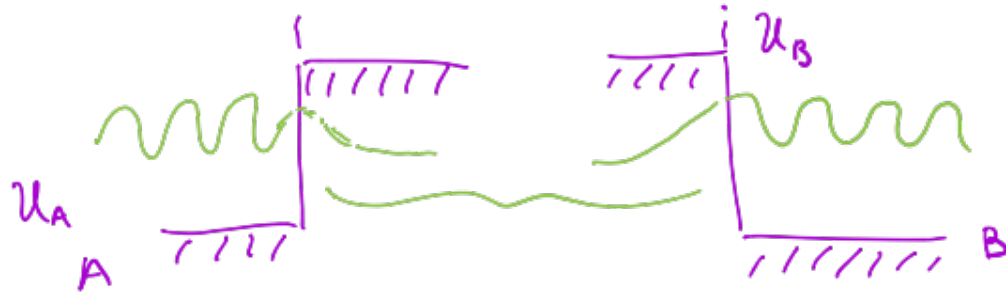
calc.

$$\text{I. } \psi(x) = A e^{\pm ikx} \quad k = \sqrt{2m(\epsilon - V)} / \hbar$$
$$\text{II. } \psi(x) = A' e^{\pm ik'x} \quad k' = \sqrt{2m(V - \epsilon)} / \hbar$$



Introduction to Tunneling

Bardeen's 1D single electron derivation and probability current



Electrode A: ψ_u / stationary states

$$i\hbar \frac{\partial \psi}{\partial t} = \left[-\frac{\hbar^2}{2m} \frac{\partial^2}{\partial z^2} + U_A \right] \psi$$

$$\psi = \psi_u e^{-iE_u t/\hbar}$$

Electrode A + B:

$$i\hbar \frac{\partial \tilde{\psi}}{\partial t} = \left[-\frac{\hbar^2}{2m} \frac{\partial^2}{\partial z^2} + U_A + U_B \right] \tilde{\psi}$$

*assume $\tilde{\psi} = \psi_u e^{-iE_u t/\hbar} + \sum_{v=1}^{\infty} c_v(t) \chi_v e^{-iE_v t/\hbar}$

Electrode B: χ_v

$$i\hbar \frac{\partial \chi_v}{\partial t} = \left[-\frac{\hbar^2}{2m} \frac{\partial^2}{\partial z^2} + U_B \right] \chi_v$$

$$\chi_v = \chi_v e^{-iE_v t/\hbar}$$

assume χ_v and ψ_u are approx orthogonal $\int \psi_u^ \chi_v d^3r = 0$
 → Trial wavefunction $\tilde{\psi}$ normalized up to order $|c_v|^2$

Introduction to Tunneling

Bardeen's 1D single electron derivation and probability current

$$\begin{aligned}
 & i\hbar \frac{\partial}{\partial t} \left[\psi_{ue} e^{-iE_u t/\hbar} + \sum_{v=1}^{\infty} c_v(t) \chi_v e^{-iE_v t/\hbar} \right] \cdot \left(-\frac{\hbar^2}{2m} \nabla^2 + U_A + U_B \right) \times \\
 & \quad \left(\psi_{ue} e^{-iE_u t/\hbar} + \sum_{v=1}^{\infty} c_v(t) \chi_v e^{-iE_v t/\hbar} \right) \\
 \Rightarrow & i\hbar \sum_{v=1}^{\infty} \frac{\partial}{\partial t} c_v(t) \chi_v e^{-iE_v t/\hbar} = U_A \sum_{v=1}^{\infty} c_v(t) \chi_v e^{-iE_v t/\hbar} + U_B \psi_{ue} e^{-iE_u t/\hbar} \\
 & i\hbar \frac{d}{dt} c_v(t) = \int_{\text{electrode } B} \psi_u U_B \chi_v^* d^3\vec{r} e^{-i(E_u - E_v)t/\hbar} \\
 & \text{(Tunneling matrix element)} \quad M_{uv} = \int_{\text{electrode } B} \psi_u U_B \chi_v^* d^3\vec{r} \\
 & I = \frac{2\pi e^2}{\hbar} \left(\sum_{uv} |M_{uv}|^2 \right) \times \\
 & \quad \rho_B(E_F) \rho_A(E_F)
 \end{aligned}$$

Introduction to Tunneling

Bardeen's 1D single electron derivation and probability current

Introduction to Tunneling

Bardeen's 1D single electron derivation and probability current

Introduction to Tunneling

Bardeen's 1D single electron derivation and probability current